



2 China

4 Shuyu Zhao¹, Tian Feng², Xuexi Tie^{1,3*}, Zebin Wang⁴

¹Key Laboratory of Aerosol Chemistry and Physics, SKLLQG, Institute of Earth Environment, Chinese Academy of Sciences, Xi'an, 710061, China

8 ²Department of Geography & Spatial Information Techniques, Ningbo University, Ningbo, 315211,
9 China

³Center for Excellence in Urban Atmospheric Environment, Institute of Urban Environment,
Chinese Academy of Sciences, Xiamen, 361021, China

12 ⁴Northwest Air Traffic Management Bureau, Civil Aviation Administration of China, Xi'an,
13 712000, China

15 Corresponding author: tiexx@ieecas.cn



17 **Key points**

18

19 The Tibetan Plateau is rapidly warming, and the temperature has risen by 2 ° C from 2013 to 2017.

20

21 The 2 ° C warming of the plateau leads to an increase in PBL height and a decrease in humidity in
22 the Sichuan Basin.

23

24 The 2 ° C warming reduces PM_{2.5} concentration in the basin by 25.1 µg m⁻³, of which primary and
25 secondary aerosols are 5.4 µg m⁻³ and 19.7 µg m⁻³, respectively.



26 **Abstract**

27

28 Impacts of global climate change on the occurrence and development of air pollution have attracted
29 more attentions. This study investigates impacts of the warming Tibetan Plateau on air quality in
30 the Sichuan Basin. Meteorological observations and ERA-interim reanalysis data reveal that the
31 Tibetan Plateau has been rapidly warming during the last 40 years (1979-2017), particularly in
32 winter when the warming rate is approximately twice as much as the annual warming rate. Since
33 2013, the winter temperature over the plateau has even risen by 2 ° C. Here, we use the WRF-CHEM
34 model to assess the impact of the 2 ° C warming on air quality in the Sichuan Basin. The model
35 results show that the 2 ° C warming causes an increase in the Planetary Boundary Layer (PBL)
36 height and a decrease in the relative humidity (RH) in the basin. The elevated PBL height
37 strengthens vertical diffusion of PM_{2.5}, while the decreased RH significantly reduces secondary
38 aerosol formation. Overall, PM_{2.5} concentration is reduced by 17.5% (~25.1 µg m⁻³), of which the
39 reduction in primary and secondary aerosols is 5.4 µg m⁻³ and 19.7 µg m⁻³, respectively. These
40 results reveal that the recent warming plateau has improved air quality in the basin, to some certain
41 extent, mitigating the air pollution therein. Nevertheless, climate system is particularly complicated,
42 and more studies are needed to demonstrate the impact of climate change on air quality in the
43 downstream regions as the plateau is likely to continue warming.

44

45 **Keywords:** climate change, air quality, Tibetan Plateau, WRF-CHEM model

46



1 Introduction

48

49 The Tibetan Plateau is known as the third pole because of its high altitude and large area. It is also
50 regarded as an important response region to the Northern Hemisphere, and even global climate due
51 to its sensitivity to climate change. Previous studies on the Tibetan Plateau show that the region was
52 experiencing warming in the second half of the 20th century, especially in the winter months (Kuang
53 and Jiao, 2016; Liu and Chen, 2000; Rangwala et al., 2009). The warming plateau not only plays a
54 significant role in driving the weather and climate change, as well as the ecological system, but also
55 has an important impact on air quality in the downstream regions. Xu et al. (2016) suggest that the
56 thermal anomaly over the Tibetan Plateau obviously increases haze frequency and surface aerosol
57 concentration in central-eastern China.

58

59 However, the impacts of climate change on air quality in China are still unclear. Some researches
60 hold the opinion that climate change induced by greenhouse gas emission increases severe haze
61 occurrence and intensity in winter at Beijing, and its impact will continue in the future (Cai et al.,
62 2017; Zou et al., 2017). Similarly, Xu et al. (2017) suggest that climate warming anomaly in the
63 lower and middle troposphere over the continent around the Yangtze River Delta leads to more haze
64 days in winter during recent decades. On the contrary, another opinion suggests that climate change
65 in the past two decades is favorable for air pollution dispersion in northern China via enhancing
66 mid-latitude cold surges in winter (Zhao et al., 2018). If cold surge is strong enough, pollutants
67 would be transported to the downstream regions, causing a better air quality in the upstream region
68 but a worse one in the downstream region. Thus, there may be regional differences in the impact of
69 climate change on air quality.

70

71 Previous studies on air pollution in China are concentrated in the developed regions, such as the
72 North China Plain, the Yangtze River Delta and the Pearl River Delta. Few studies have paid
73 attention to the Sichuan Basin, although the region is undergoing severe air pollution, and mean
74 PM_{2.5} concentration is more than 110 µg m⁻³ in winter (Qiao et al., 2019; Tao et al., 2017; Wang et



75 al., 2018; Yang et al., 2011). Thus, it is necessary to explore the underlying causes that leads to air
76 pollution in the Sichuan Basin.

77

78 The Sichuan Basin locates in the downstream region of the Tibetan Plateau, and its weather
79 conditions are obviously affected by the plateau (Duan et al., 2012; Hua, 2017; Zhao et al., 2019).
80 For instance, the foggy weather, southwest vortex and low-level shear line over the basin are closely
81 associated with the plateau (Zhu et al., 2000). These changes in weather conditions induced by the
82 plateau undoubtedly affect the development and dispersion of air pollution in the basin, because the
83 huge terrain can trigger a thermodynamic forcing, which is of great importance for weather
84 conditions in the surrounding regions (Bei et al., 2016; 2017; Zhao et al., 2015).

85

86 This study therefore focuses on how climate change on the Tibetan Plateau affects air quality in the
87 Sichuan Basin in recent years. Section 3 analyzes the climate change on the Tibetan Plateau in the
88 past four decades, and especially emphasizes the change in recent five years. In Section 4, we design
89 two numerical simulations to calculate the impact of climate change on air quality. One is a baseline
90 simulation, which is constrained by observed surface meteorological parameters and pollutant
91 concentrations. The other is a sensitivity simulation, which uses the same emission inventory and
92 meteorological fields as the baseline simulation except for the changed air temperature. We compare
93 the difference of PM_{2.5} concentrations in these two cases, and also calculate the differences in
94 meteorological parameters that include winds (wind speed and direction), air temperature, and
95 relative humidity (RH), as well as the Planetary Boundary Layer (PBL) height. Based on the
96 differences in PM_{2.5} concentration and meteorological parameters above, we finally explain the
97 cause-to-effect relationship between climate change on the Tibetan Plateau and the changes in the
98 PBL height and RH in the Sichuan Basin. Moreover, we calculate the effect of the relationship on
99 air quality in the Sichuan Basin.

100

101 **2 Data and Methods**

102



103 **2.1 Observations**

104

105 To ensure a robust result, we use two datasets of surface air temperature in this study. One is the
106 European Center for Medium-Range Weather Forecasts (ECMWF) ERA-Interim monthly mean
107 reanalysis data (1979-2018), obtained from the website of <http://apps.ecmwf.int/datasets/>, with the
108 finest horizontal resolution of $0.125^{\circ} \times 0.125^{\circ}$. The other is hourly and monthly mean weather-station
109 observations from the National Oceanic and Atmospheric Administration (NOAA), which is
110 available on the website of
111 <http://gis.ncdc.noaa.gov/map/viewer/#app=clim&cfg=cdo&theme=hourly&layers=1&node=gis>.

112

113 Figure 1 shows the distribution of weather stations over the Tibetan Plateau, and these weather
114 stations widely cover the entire plateau. Trends of annual mean and winter surface air temperature
115 over the plateau are analyzed, and the winter is averaged over 3-month periods (December-January-
116 February). Additionally, we use ambient air quality data to validate the model performance. Since
117 2013, the data are released by Ministry of Environmental Protection, China at
118 <http://www.aqistudy.cn/>, including hourly PM_{2.5}, CO, and O₃ mass concentrations. The monitoring
119 stations for air quality are also shown in Figure 1.

120

121 **2.2 Model configuration and experiments**

122

123 A state-of-the-art regional dynamical and chemical model (WRF-CHEM model) is used in the
124 study. The simulation domain covers the Tibetan Plateau and the Sichuan Basin (Figure 1). The
125 Tibetan Plateau covers about 2.5 million km², with the averaged elevation of 4500 m, and the
126 Sichuan Basin covers about 0.16 million km², with the elevation in the center of the basin less than
127 1000 m (250 - 700 m). The model is set by a horizontal grid resolution of 9 km (451 × 221 grids),
128 with 35 vertical sigma levels. The model description in detail is seen by Grell et al. (2005). The
129 evaluation of the model performance has been conducted by many previous studies (Li et al., 2011a;
130 Tie et al., 2009; 2007). In this study, we use the Goddard longwave and shortwave radiation



parameterization (Dudhia, 1989), the WSM 6-class graupel microphysics scheme (Hong and Lim, 2006), the Mellor-Yamada-Janji (MYJ) planetary boundary layer scheme (Janjić, 2002), the unified Noah land-surface model (Chen and Dudhia, 2001) and Monin-Obukhov surface layer scheme (Janjić, 2002). For chemical schemes, we use a new flexible gas-phase chemical module and the Community Multiscale Air Quality (CMAQ, version 4.6) aerosol module developed by the US EPA (Binkowski, 2003). Gas-phase atmospheric reactions of volatile organic compounds (VOCs) and nitrogen oxide (NO_x) use the SAPRC-99 (Statewide Air Pollution Research Center, version 1999) chemical mechanism. Inorganic aerosols use the ISORROPIA version 1.7, referring to Li et al. (2011a) and Feng et al. (2016). A SO₂ heterogeneous reaction mechanism on aerosol surfaces involving aerosol water is added (Li et al., 2017a), and NO₂ heterogeneous reaction to produce HONO is also considered (Li et al., 2010). The secondary organic aerosol (SOA) calculation uses a non-traditional volatility basis-set approach by Li et al. (2011b). The photolysis rates are calculated by a fast Tropospheric Ultraviolet and Visible (FTUV) radiation transfer model, in which the impacts of aerosols and clouds on the photochemistry processes are considered (Li et al., 2011a; Tie et al., 2003; 2005). The wet deposition is calculated by the method used in CMAQ and the dry deposition follows Wesely (1989).

We use the MIX anthropogenic emission inventory for the year of 2010, and it is available at Multi-resolution Emission Inventory for China (<http://www.meicmodel.org/dataset-mix.html>), consisting of industrial, power, transportation, and agricultural as well as residential sources (Li et al., 2017b; Zhang et al., 2009). Here, we use a ‘top-down’ method to constrain the emission inventory via comparing the simulations with the measurements. The biogenic emissions are online calculated by the Model of Emissions of Gases and Aerosol from Nature (MEGAN) (Guenther et al., 2006). Initial and boundary meteorological fields in the model are driven by 6-hour 1° × 1° NCEP (National Centers for Environmental Prediction) reanalysis data. Chemical lateral conditions are provided by a global chemistry transport model – MOZART (Model for Ozone And Related chemical Tracer, version 4), with a 6-h output (Emmons et al., 2010; Tie et al., 2005). The spin-up time of the WRF-CHEM model is 1 day.



159

160 Two numerical experiments are performed. One is the baseline simulation in the 2013-2014 winter
161 (January 2014), and the other is a sensitivity simulation that has an observational increase in air
162 temperature over the Tibetan Plateau. In other words, the sensitivity simulation uses the same
163 emission inventory and meteorological conditions as the baseline simulation except that the
164 temperature fields over the Tibetan Plateau are changed. We set the temperature increment to 2°C
165 in the sensitivity simulation, because observational temperature increment in winter is about 2°C
166 from 2013 to 2017 (Table S1). Comparing the difference between the sensitivity simulation and
167 the baseline simulation, we calculate the impact of the warming Tibetan Plateau on air quality in
168 the Sichuan Basin.

169

170 **3 The warming Tibetan Plateau in the last four decades**

171

172 Figure 2 shows the variability and linear trend of surface air temperature at 10 weather stations
173 over the Tibetan Plateau in winter during the last four decades (1979 - 2017). The winter mean
174 temperature recorded from all the weather stations exhibits an obvious annual fluctuation and the
175 linear regression shows a significant rising trend. Clearly, the plateau is continuously undergoing
176 a warming phase, albeit with regional differences in the warming magnitude. The warming rates
177 in different regions vary in the range of 0.5 - 1.0°C decade⁻¹. Compared with the warming rate of
178 annual mean temperature (Figure S1), the warming rate in winter is approximately twice as much,
179 suggesting that the warming in winter is more significant.

180

181 Using the ERA-interim reanalysis data, Figure 3 shows the temperature change during the same
182 period (1979 - 2017). The result is consistent with weather records, showing that air temperature
183 is significantly rising in most parts of the plateau. The maximal warming rate is around 0.6 - 0.8°C
184 decade⁻¹, appeared in the central and southern plateau. The warming in the rest areas is slighter,
185 with a rate of 0.3 - 0.6 °C decade⁻¹. Particularly, the averaged warming rate in the vast central
186 plateau reaches about 1.0°C yr⁻¹ in recent five years (Figure S2), greater than the warming rate



187 during the entire 40 years (Figure 3). Both the observation records and reanalysis data evidently
188 show that the plateau has been warming in the last four decades, and also the warming trend for
189 recent years is more significant.

190

191 From the above temperature change analysis, we notice that there is obviously a positive
192 temperature anomaly between 2013 and 2017 winters, implying for an accelerating warming over
193 the plateau. The observational temperature in winter increases by about 2°C between 2013 and
194 2017. Therefore, the impact of the 2°C warming on air quality in the Sichuan Basin is investigated.
195 In order to isolatedly assess the effect of a rapid temperature increase and to eliminate the effect of
196 other factors, a sensitivity study using the WRF-CHEM model is conducted for considering the
197 2°C temperature increase from the value in 2013 (see Figure 2 and Table S1).

198

199 **4 Results and Discussion**

200

201 **4.1 Model validation**

202

203 To systemically evaluate the model performance on simulation O₃, CO and PM_{2.5} mass
204 concentrations, three statistical indices are used. They are the mean bias (MB), root mean square
205 error (RMSE), and index of agreement (IOA). The calculation formulas are given in Text S1. The
206 IOAs of air temperature and RH are 0.85 and 0.79, respectively (Figure S3), suggesting that the
207 model well captures the diurnal cycle of temperature and the variability of RH. However, the
208 calculated wind speed is overestimated, especially in the region between the Tibetan Plateau and
209 the Sichuan Basin. This is because there is a dramatic elevation drop in the region, which makes it
210 difficult for the model to replicate the observed wind speed and direction.

211

212 Figure 4 shows comparisons of hourly O₃, CO and PM_{2.5} concentrations between the model
213 simulations and measurements. The result shows that the simulated CO mean level is close to the
214 measurement, with a MB of 0.11 mg m⁻³, indicating that the model reasonably reproduces the



215 meteorological fields and long-range transport. Because the chemical lifetime of CO is relatively
 216 long (~months), the variability of CO is dominantly determined by the meteorological fields and
 217 atmospheric transport process. For the simulation of O₃, in addition to the effects of meteorological
 218 fields and atmospheric transport process, its variability is strongly controlled by the photochemical
 219 process. The model result shows that the simulated diurnal cycle of O₃ is reasonably agreed with
 220 the measurement, with an IOA of 0.79. There is only a small bias between the simulated and
 221 measured O₃ mean concentration. The simulated O₃ concentration is 1.7 µg m⁻³ higher than the
 222 measurement, suggesting that both the photochemistry and long-range transport well capture the O₃
 223 variability in the region. Finally, the IOA between the simulated and measured PM_{2.5} concentrations
 224 is 0.80, indicating that the aerosol module in the model generally captures the measured PM_{2.5}
 225 variation.

226
 227 However, there are some noticeable discrepancies between the simulations and the measurements.
 228 For instance, the simulated magnitude of PM_{2.5} concentration is larger than the measurement, and
 229 its mean level is underestimated by 13.1 µg m⁻³, less than 10% of the measurement (~153.5 µg m⁻³).
 230 These discrepancies are likely due to the biases in the uncertainties in emission inventory and
 231 small-scale dynamical fields. During the period of Jan 17th to Jan 20th, the overestimated PM_{2.5}
 232 concentration is mainly caused by the overestimated wind speed and the departure of wind direction
 233 (Figure S3). This is also shown by the overestimation of CO concentration because the observed
 234 northwest wind is not well simulated due to the complicated topography.

235

236 4.2 Change in winter PM_{2.5} concentration over the basin

237

238 To examine impacts of the warming plateau on PM_{2.5} concentration in winter in the Sichuan Basin,
 239 the time series of PM_{2.5} concentrations in the two case simulations (i.e., with and without the 2°C
 240 warming over the plateau) are respectively calculated (Figure 5). The results show that PM_{2.5}
 241 concentration in the basin is significantly reduced by an average of 25.1 µg m⁻³ in the case of 2°C
 242 warming. The maximum hourly reduction reaches to 84.6 µg m⁻³ (Figure S4a) and the maximum



percentage reduction is about 64.5% (Figure S4b). Interestingly, the maximum reduction always occurs while $PM_{2.5}$ concentration reaches a peak value, which suggests that the impact of the warming plateau is extremely significant during the period of high $PM_{2.5}$ concentration. This result is similar to previous studies which also point out that extreme weather plays important roles in affecting air quality (De Sario et al., 2013; Hong et al., 2019; Tsangari et al., 2016; Zhang et al., 2016). That is to say, the impact of the warming plateau on air quality is apt to be amplified in extremely high $PM_{2.5}$ concentrations.

To better understand the impact of the warming plateau on $PM_{2.5}$ concentration in the Sichuan Basin, we also calculate the changes in $PM_{2.5}$ chemical composition in the basin (Figure 6). As a result, secondary aerosol reduces by $19.7 \mu g m^{-3}$, accounting for 78.5% of the total reduction. For example, the largest reduction is SOA, reducing from $23.2 \mu g m^{-3}$ in the base case to $10.8 \mu g m^{-3}$ in the warming case. The second reduction is sulfate ($31.8 \mu g m^{-3}$ in the base case and $28.6 \mu g m^{-3}$ in the warming case). The next are nitrate and ammonium ($22.3 \mu g m^{-3}$ and $19.1 \mu g m^{-3}$ in the base case, and $20.2 \mu g m^{-3}$ and $17.5 \mu g m^{-3}$ in the warming case).

There are also significant changes in the spatial distribution of $PM_{2.5}$ concentration. Figure 7 shows the spatial distribution of changes in surface $PM_{2.5}$ concentration and winds after $2^{\circ}C$ warming over the plateau. Apparently, there is a larger decrease in $PM_{2.5}$ concentration in the whole basin, and the maximum reduction is more than $30 \mu g m^{-3}$. By contrast, $PM_{2.5}$ concentration increases by $5 - 15 \mu g m^{-3}$ at the eastern edge of the plateau. Wind patterns show that easterly winds over the basin enhance while westerly wind over the plateau weaken (Figure S5 and Figure 7). Enhanced easterly winds cause an increased transport of $PM_{2.5}$ from the basin to the plateau. Moreover, weakened westerly winds convergent with enhanced easterly winds on the border between the plateau and the basin, jointly leading to an increase in $PM_{2.5}$ concentration at the eastern edge of the plateau. Additionally, northerly winds over the basin slightly enhance, conducive to diluting the air and reducing $PM_{2.5}$ concentration. Thus, easterly winds transport and northerly winds dilution are both favorable for a reduction of $PM_{2.5}$ concentration in the basin. In addition to the wind effect, there are also other



important factors to produce the $\text{PM}_{2.5}$ reduction in the basin, such as the PBL height and RH, which will be analyzed as follows.

4.3 Impact of PBL height on $\text{PM}_{2.5}$ concentration

Previous studies show that the PBL development plays an important role in diffusing pollutants (Miao et al., 2017; Su et al., 2018; Tie et al., 2015). Here we calculate the change in the PBL height due to the 2°C warming over the plateau, and then analyze the effect of the change in PBL height on $\text{PM}_{2.5}$ concentration in the basin.

Our results suggest that the 2°C warming plays different roles in the PBL development over the plateau and the basin. Due to the 2°C warming, the PBL height decreases in most areas of the plateau, but rises by 50 - 200 m over the basin (Figure 8). As known, a shallow PBL constrains $\text{PM}_{2.5}$ near the surface via suppressing vertical dispersion (Fan et al., 2011; Iversen, 1984). Conversely, a deep PBL is favorable for $\text{PM}_{2.5}$ diffusion. Thus, we explore the underlying cause that leads to the difference in the PBL height over the plateau and the basin. Figure 9 shows that vertical profiles of changes in temperature and winds in the plateau and the basin, because the PBL height is strongly related to the changes in vertical temperature and wind. The results show that the 2°C warming causes a maximum warm layer around 1 km above the ground of the plateau. Interestingly, the warm layer acts as a dome covering 4.5 km above the Sichuan Basin (Figure 9a). Xu et al. (2017) also finds out a significant warm plume extending from the plateau to the downstream Sichuan Basin and Yangtze River Delta by use of NCEP/NCAR reanalysis data. This is closely associated with a sharp topography decrease (from ~ 5 km in the plateau to < 1 km in the basin). In the basin, there is a decrease in the temperature from the surface to ~ 4 km, with a maximal temperature reduction ($1 - 2^\circ\text{C}$) located at 1.5 km to 3 km above the ground (Figure 9a). As a result, the vertical temperature gradient increases and the instability also increases in the lower troposphere of the basin, thereby causing a higher PBL height than that in the non-warming case (Figure 9b). On the contrary, the change in vertical temperature profile leads to a decreased vertical temperature gradient and



299 increased thermal stability in the lower troposphere of the plateau, so the PBL height decreases in
300 the region.

301

302 Moreover, the 2°C warming reduces the zonal temperature gradient from the plateau to the basin,
303 which causes a weakened westerly wind over the plateau. Meanwhile, the east wind strengthens in
304 the basin. The weakened westerly wind and the strengthened east wind converge on the east side of
305 the plateau, triggering an ascending motion. The mechanism of the ascending motion is similar to
306 the plateau “heat pump” effect that implies for a warm updraft forced by a heating plateau (Lau et
307 al., 2006). Thus, both the ascending motion at the eastern edge of the plateau and the east wind in
308 the basin strengthen, which is favorable for the development of the PBL. The elevated PBL
309 facilitates vertical diffusion, leading to a reduction in $PM_{2.5}$ concentration over the basin.
310 Additionally, the updraft enhances the $PM_{2.5}$ transport from the basin to the plateau, which also
311 leads to a decrease in $PM_{2.5}$ concentration over the basin.

312

313 **4.4 Effect of RH on $PM_{2.5}$ concentration**

314

315 In addition to the PBL height, ambient RH is a key factor for secondary aerosol formation (Tie et
316 al., 2017; Wang et al., 2016). Previous studies indicate that aerosol hygroscopic growth cannot
317 occurs until the humidity exceeds 50% (Liu et al., 2008). When the humidity is greater than 60%,
318 hygroscopic growth factor of urban aerosol increases significantly with humidity (Liu et al., 2008).

319

320 Figure 10 shows that there is remarkable change in RH in the basin due to the 2°C warming of the
321 plateau. In the baseline simulation, the RH varies in the range of 40% - 80% over the basin (Figure
322 10a). However, the RH varies from 40% to 70% in the 2 °C warming simulation (Figure 10b),
323 suggesting that the basin becomes drier when the plateau is warmer.

324

325 The RH comparison between these two numerical simulations reveals that the 2 °C warming causes
326 a 2.5% - 10% decrease in the RH over the basin (Figure 11). This change in RH has a critical effect
327 on the secondary aerosol formation. As explained by Tie et al. (2017), the reduction of RH



(especially during the stage of RH from 80% to 70%) causes a significant decrease of hygroscopic growth on the aerosol surface, resulting in less water surface for producing secondary aerosol, such as sulfate and nitrate. As a result, the $\text{PM}_{2.5}$ concentration decreases in the basin. There are also some fingerprints of the RH's effect on $\text{PM}_{2.5}$ concentration. Firstly, the spatial distributions of RH reduction and $\text{PM}_{2.5}$ concentration reduction have similar patterns (Figure 11 and Figure 7), and the region with more humidity decrease overlaps the region with more $\text{PM}_{2.5}$ decreases. Secondly, as shown in Figure 6, the changes in $\text{PM}_{2.5}$ compositions indicate that the reduced $\text{PM}_{2.5}$ concentration is mainly caused by the decrease in secondary aerosol concentration. Therefore, the RH change plays an important role for $\text{PM}_{2.5}$ concentration in the basin.

337

338 5 Conclusions

339

ERA-interim reanalysis data and observation records at 10 weather stations show that the Tibetan Plateau is significantly warming during the past four decades (1979-2017), particularly in winter. The temperature increase rate is $0.5^{\circ}\text{C decade}^{-1}$ to $1.0^{\circ}\text{C decade}^{-1}$ in winter, approximately twice as much as the increase rate of annual mean temperature. In recent 5 years (2013-2017), the central plateau is significantly warming with an increase rate of $1.0^{\circ}\text{C yr}^{-1}$, encompassing the warming rate during the entire 40 years. Rapid warming has caused the winter temperature to increase by an average of 2°C over the entire plateau from 2013 to 2017.

347

The WRF-Chem model is used to assess the impact of 2°C warming of the plateau on air quality over the downstream Sichuan Basin. The most significant impact of the 2°C warming on $\text{PM}_{2.5}$ concentration in the basin is via reducing relative humidity and increasing PBL height. A lower ambient humidity decreases aerosol hygroscopic growth, which weakens secondary aerosol formation and leads to a significant reduction in secondary aerosol concentration. Moreover, the 2°C warming induces an increase in vertical temperature gradient over the basin, strengthening turbulence mixing and elevating PBL height. The elevated PBL height is favorable for vertical diffusion that causes a reduction of $\text{PM}_{2.5}$ in the basin. Additionally, the uplift effect by an enhanced



356 ascending motion at the eastern edge of the plateau also contributes to PM_{2.5} reduction within the
357 basin.

358

359 In summary, the 2°C warming over the plateau in recent five years comprehensively induces a rising
360 PBL height and a drying ambient air over the basin, which greatly reduces PM_{2.5} secondary
361 compositions. On average, PM_{2.5} concentration reduces by 25.1 µg m⁻³, of which the primary and
362 secondary aerosols decrease by 5.4 µg m⁻³ and 19.7 µg m⁻³, respectively. Since the plateau is likely
363 to continue warming, in-depth understanding to climate change on the Tibetan Plateau is required.
364 Long-term PM_{2.5} monitoring is also needed to validate the impact of the warming plateau on air
365 quality.

366

367 *Data availability.* The data used in this study are available from the corresponding author upon
368 request (tiexx@ieecas.cn).

369 *Supplement.* Supplemental materials to this article can be found online at <http://xxxxxx>

370 *Author contributions.* XX designed research, and revised the final paper. SY performed research,
371 and wrote the paper. XX and SY provided financial support. TF validated the model, modified the
372 chart code and reviewed the paper. ZB collected and analyzed the weather-stations data.

373 *Competing interests.* The authors declare that they have no conflict of interest.

374 *Acknowledgements.* This work is supported by the National Natural Science Foundation of China
375 (Nos. 41430424, 41730108 and 41807307) and the West Light Foundation of the Chinese Academy
376 of Sciences (Nos. XAB2016B04). We also would like to acknowledge European Center for
377 Medium-Range Weather Forecasts (ERA-interim) for reanalysis data which are freely obtained by
378 a following registration on the website <http://apps.ecmwf.int/datasets/>. Ambient weather-station
379 observations are obtained from the National Oceanic and Atmospheric Administration (NOAA),
380 <http://gis.ncdc.noaa.gov/map/viewer/#app=clim&cfg=cdo&theme=hourly&layers=1&node=gis>.
381 The hourly ambient surface O₃, CO and PM_{2.5} mass concentrations are real-timely released by
382 Ministry of Environmental Protection, China on the website <http://www.aqistudy.cn/>, freely
383 downloaded from <http://106.37.208.233:20035/>. The MEIC-2012 (Multi-resolution Emission
384 Inventory for China) anthropogenic emission inventory is available on the website,
385 <http://www.meicmodel.org>. The authors also thank anonymous reviewers for their helpful
386 comments and suggestions.



387 Reference

388

389 Bei, N., Li, G., Huang, R.-J., Cao, J., Meng, N., Feng, T., Liu, S., Zhang, T., Zhang, Q. and Molina,
 390 L. T.: Typical synoptic situations and their impacts on the wintertime air pollution in the Guanzhong
 391 basin, China, *Atmos. Chem. Phys.*, 16(11), 7373–7387, doi:10.5194/acp-16-7373-2016, 2016.

392 Bei, N., Zhao, L., Xiao, B., Meng, N. and Feng, T.: Impacts of local circulations on the wintertime
 393 air pollution in the Guanzhong Basin, China, *Science of The Total Environment*, 592, 373–390,
 394 doi:10.1016/j.scitotenv.2017.02.151, 2017.

395 Binkowski, F. S.: Models-3 Community Multiscale Air Quality (CMAQ) model aerosol component
 396 1. Model description, *J. Geophys. Res.*, 108(D6), 2981, doi:10.1029/2001JD001409, 2003.

397 Cai, W., Li, K., Liao, H., Wang, H. and Wu, L.: Weather conditions conducive to Beijing severe
 398 haze more frequent under climate change, *Nat. Clim. Change*, 7(4), 257–262,
 399 doi:10.1038/nclimate3249, 2017.

400 Chen, F. and Dudhia, J.: Coupling an Advanced Land Surface–Hydrology Model with the Penn
 401 State–NCAR MM5 Modeling System. Part I: Model Implementation and Sensitivity, *Mon. Weather*
 402 *Rev.*, 129(4), 569–585, doi:10.1175/1520-0493(2001)129<0569:CAALSH>2.0.CO;2, 2001.

403 De Sario, M., Katsouyanni, K. and Michelozzi, P.: Climate change, extreme weather events, air
 404 pollution and respiratory health in Europe, *Eur Respir J*, 42(3), 826–843,
 405 doi:10.1183/09031936.00074712, 2013.

406 Duan, A., Wu, G., Liu, Y., Ma, Y. and Zhao, P.: Weather and climate effects of the Tibetan Plateau,
 407 *Adv. in Atmos. Sci.*, 29(5), 978–992, doi:10.1007/s00376-012-1220-y, 2012.

408 Dudhia, J.: Numerical Study of Convection Observed during the Winter Monsoon Experiment
 409 Using a Mesoscale Two-Dimensional Model, *J. Atmos. Sci.*, 46(20), 3077–3107, doi:10.1175/1520-
 410 0469(1989)046<3077:NSOCOD>2.0.CO;2, 1989.

411 Emmons, L. K., Walters, S., Hess, P. G., Lamarque, J. F., Pfister, G. G., Fillmore, D., Granier, C.,
 412 Guenther, A., Kinnison, D., Laepple, T., Orlando, J., Tie, X., Tyndall, G., Wiedinmyer, C.,
 413 Baughcum, S. L. and Kloster, S.: Description and evaluation of the Model for Ozone and Related
 414 chemical Tracers, version 4 (MOZART-4), *Geosci. Model Dev.*, 3(1), 43–67, doi:10.5194/gmd-3-
 415 43-2010, 2010.

416 Fan, S. J., Fan, Q., Yu, W., Luo, X. Y., Wang, B. M., Song, L. L. and Leong, K. L.: Atmospheric
 417 boundary layer characteristics over the Pearl River Delta, China, during the summer of 2006:
 418 measurement and model results, *Atmos. Chem. Phys.*, 11(13), 6297–6310, doi:10.5194/acp-11-
 419 6297-2011, 2011.

420 Feng, T., Li, G., Cao, J., Bei, N., Shen, Z., Zhou, W., Liu, S., Zhang, T., Wang, Y., Huang, R.-J.,



- 421 Tie, X. and Molina, L. T.: Simulations of organic aerosol concentrations during springtime in the
 422 Guanzhong Basin, China, *Atmos. Chem. Phys.*, 16(15), 10045–10061, doi:10.5194/acp-16-10045-
 423 2016, 2016.
- 424 Grell, G. A., Peckham, S. E., Schmitz, R., McKeen, S. A., Frost, G., Skamarock, W. C. and Eder,
 425 B.: Fully coupled “online” chemistry within the WRF model, *Atmos. Environ.*, 39(37), 6957–6975,
 426 doi:10.1016/j.atmosenv.2005.04.027, 2005.
- 427 Guenther, A., Karl, T., Harley, P., Wiedinmyer, C., Palmer, P. I. and Geron, C.: Estimates of global
 428 terrestrial isoprene emissions using MEGAN (Model of Emissions of Gases and Aerosols from
 429 Nature), *Atmos. Chem. Phys.*, 6(11), 3181–3210, doi:10.5194/acp-6-3181-2006, 2006.
- 430 Hong, C., Zhang, Q., Zhang, Y., Davis, S. J., Tong, D., Zheng, Y., Liu, Z., Guan, D., He, K. and
 431 Schellnhuber, H. J.: Impacts of climate change on future air quality and human health in China, *P.*
 432 *Natl. Acad. Sci. USA*, 116(35), 17193–17200, doi:10.1073/pnas.1812881116, 2019.
- 433 Hong, S.-Y. and Lim, J.-O. J.: The WRF single-moment 6-class microphysics scheme (WSM6), *J.*
 434 *Korean Meteor. Soc.*, 42(2), 129–151, 2006.
- 435 Hua, M.: Analysis and simulation study on the influence of heat condition over Qinghai-Xizang
 436 Plateau on climate over South-West China, *Plateau Meteorology*, 22, 152–156, 2017.
- 437 Iversen, T.: On the atmospheric transport of pollution to the Arctic, *Geophys. Res. Lett.*, 11(5), 457–
 438 460, doi:10.1029/GL011i005p00457, 1984.
- 439 Janjić, Z. I.: Nonsingular implementation of the Mellor-Yamada level 2.5 scheme in the NCEP meso
 440 model, Camp Springs, MD. 2002.
- 441 Kuang, X. and Jiao, J. J.: Review on climate change on the Tibetan Plateau during the last half
 442 century, *J. Geophys. Res.*, 1–29, doi:10.1002/(ISSN)2169-8996, 2016.
- 443 Lau, K. M., Kim, M. K. and Kim, K. M.: Asian summer monsoon anomalies induced by aerosol
 444 direct forcing: the role of the Tibetan Plateau, *Clim. Dynam.*, 26(7-8), 855–864,
 445 doi:10.1007/s00382-006-0114-z, 2006.
- 446 Li, G., Bei, N., Cao, J., Huang, R., Wu, J., Feng, T., Wang, Y., Liu, S., Zhang, Q., Tie, X. and
 447 Molina, L. T.: A possible pathway for rapid growth of sulfate during haze days in China, *Atmos.*
 448 *Chem. Phys.*, 17(5), 3301–3316, doi:10.5194/acp-17-3301-2017, 2017a.
- 449 Li, G., Bei, N., Tie, X. and Molina, L. T.: Aerosol effects on the photochemistry in Mexico City
 450 during MCMA-2006/MILAGRO campaign, *Atmos. Chem. Phys.*, 11(11), 5169–5182,
 451 doi:10.5194/acp-11-5169-2011, 2011a.
- 452 Li, G., Lei, W., Zavala, M., Volkamer, R., Dusanter, S., Stevens, P. and Molina, L. T.: Impacts of
 453 HONO sources on the photochemistry in Mexico City during the MCMA-2006/MILAGO
 454 Campaign, *Atmos. Chem. Phys.*, 10(14), 6551–6567, doi:10.5194/acp-10-6551-2010, 2010.



- 455 Li, G., Zavala, M., Lei, W., Tsimpidi, A. P., Karydis, V. A., Pandis, S. N., Canagaratna, M. R. and
 456 Molina, L. T.: Simulations of organic aerosol concentrations in Mexico City using the WRF-CHEM
 457 model during the MCMA-2006/MILAGRO campaign, *Atmos. Chem. Phys.*, 11(8), 3789–3809,
 458 doi:10.5194/acp-11-3789-2011, 2011b.
- 459 Li, M., Zhang, Q., Kurokawa, J.-I., Woo, J.-H., He, K., Lu, Z., Ohara, T., Song, Y., Streets, D. G.,
 460 Carmichael, G. R., Cheng, Y., Hong, C., Huo, H., Jiang, X., Kang, S., Liu, F., Su, H. and Zheng,
 461 B.: MIX: a mosaic Asian anthropogenic emission inventory under the international collaboration
 462 framework of the MICS-Asia and HTAP, *Atmos. Chem. Phys.*, 17(2), 935–963, doi:10.5194/acp-
 463 17-935-2017, 2017b.
- 464 Liu, X. and Chen, B.: CLIMATIC WARMING IN THE TIBETAN PLATEAU DURING RECENT
 465 DECADES, *Int. J. Climatol.*, 20, 1729–1742, 2000.
- 466 Liu, X., Cheng, Y., Zhang, Y., Jung, J., Sugimoto, N., Chang, S.-Y., Kim, Y. J., Fan, S. and Zeng,
 467 L.: Influences of relative humidity and particle chemical composition on aerosol scattering
 468 properties during the 2006 PRD campaign, *Atmos. Environ.*, 42(7), 1525–1536,
 469 doi:10.1016/j.atmosenv.2007.10.077, 2008.
- 470 Miao, Y., Guo, J., Liu, S., Liu, H., Li, Z., Zhang, W. and Zhai, P.: Classification of summertime
 471 synoptic patterns in Beijing and their associations with boundary layer structure affecting aerosol
 472 pollution, *Atmos. Chem. Phys.*, 17(4), 3097–3110, doi:10.5194/acp-17-3097-2017, 2017.
- 473 Qiao, X., Guo, H., Tang, Y., Wang, P., Deng, W., Zhao, X., Hu, J., Ying, Q. and Zhang, H.: Local
 474 and regional contributions to fine particulate matter in the 18 cities of Sichuan Basin, southwestern
 475 China, *Atmos. Chem. Phys.*, 19(9), 5791–5803, doi:10.5194/acp-19-5791-2019, 2019.
- 476 Rangwala, I., Miller, J. R. and Xu, M.: Warming in the Tibetan Plateau: Possible influences of the
 477 changes in surface water vapor, *Geophys. Res. Lett.*, 36(6), 5–6, doi:10.1029/2009GL037245, 2009.
- 478 Su, T., Li, Z. and Kahn, R.: Relationships between the planetary boundary layer height and surface
 479 pollutants derived from lidar observations over China: regional pattern and influencing factors,
 480 *Atmos. Chem. Phys.*, 18(21), 15921–15935, doi:10.5194/acp-18-15921-2018, 2018.
- 481 Tao, J., Zhang, L., Cao, J. and Zhang, R.: A review of current knowledge concerning PM
 482 2.5 chemical composition, aerosol optical properties and their relationships across China, *Atmos.*
 483 *Chem. Phys.*, 17(15), 9485–9518, doi:10.5194/acp-17-9485-2017, 2017.
- 484 Tie, X., Huang, R.-J., Cao, J., Zhang, Q., Cheng, Y., Su, H., Di Chang, schl, U. P. X., Hoffmann,
 485 T., Dusek, U., Li, G., Worsnop, D. R. and Dowd, C. D. O. X.: Severe Pollution in China Amplified
 486 by Atmospheric Moisture, *Sci. Rep.*, 1–8, doi:10.1038/s41598-017-15909-1, 2017.
- 487 Tie, X., Madronich, S., Li, G., Ying, Z., Weinheimer, A., Apel, E. and Campos, T.: Simulation of
 488 Mexico City plumes during the MIRAGE-Mex field campaign using the WRF-Chem model, *Atmos.*
 489 *Chem. Phys.*, 9(14), 4621–4638, doi:10.5194/acp-9-4621-2009, 2009.



- 490 Tie, X., Madronich, S., Li, G., Ying, Z., Zhang, R., Garcia, A. R., Lee-Taylor, J. and Liu, Y.:
 491 Characterizations of chemical oxidants in Mexico City: A regional chemical dynamical model
 492 (WRF-Chem) study, *Atmos. Environ.*, 41(9), 1989–2008, doi:10.1016/j.atmosenv.2006.10.053,
 493 2007.
- 494 Tie, X., Madronich, S., Walters, S., Zhang, R., Rasch, P. and Collins, W.: Effect of clouds on
 495 photolysis and oxidants in the troposphere, *J. Geophys. Res.*, 108(D20), 4642,
 496 doi:10.1029/2003JD003659, 2003.
- 497 Tie, X., Sasha, M., Stacy, W., David, E., Paul, G., Natalie, M., Renyi, Z., Lou, C. and Guy, B.:
 498 Assessment of the global impact of aerosols on tropospheric oxidants, *J. Geophys. Res.*,
 499 110(D03204), 13,791, doi:10.1029/2004JD005359, 2005.
- 500 Tie, X., Zhang, Q., He, H., Cao, J., Han, S., Gao, Y., Li, X. and Jia, X. C.: A budget analysis of the
 501 formation of haze in Beijing, *Atmos. Environ.*, 100, 25–36, doi:10.1016/j.atmosenv.2014.10.038,
 502 2015.
- 503 Tsangari, H., Paschalidou, A. K., Kassomenos, A. P., Vardoulakis, S., Heaviside, C., Georgiou, K.
 504 E. and Yamasaki, E. N.: Extreme weather and air pollution effects on cardiovascular and respiratory
 505 hospital admissions in Cyprus, *Science of The Total Environment*, 542(Part A), 247–253,
 506 doi:10.1016/j.scitotenv.2015.10.106, 2016.
- 507 Wang, G., Zhang, R., Gomez, M. E., Yang, L., Levy Zamora, M., Hu, M., Lin, Y., Peng, J., Guo,
 508 S., Meng, J., Li, J., Cheng, C., Hu, T., Ren, Y., Wang, Y., Gao, J., Cao, J., An, Z., Zhou, W., Li, G.,
 509 Wang, J., Tian, P., Marrero-Ortiz, W., Secrest, J., Du, Z., Zheng, J., Shang, D., Zeng, L., Shao, M.,
 510 Wang, W., Huang, Y., Wang, Y., Zhu, Y., Li, Y., Hu, J., Pan, B., Cai, L., Cheng, Y., Ji, Y., Zhang,
 511 F., Rosenfeld, D., Liss, P. S., Duce, R. A., Kolb, C. E. and Molina, M. J.: Persistent sulfate formation
 512 from London Fog to Chinese haze, *P. Natl. Acad. Sci. USA*, 113(48), 13630–13635,
 513 doi:10.1073/pnas.1616540113, 2016.
- 514 Wang, H., Tian, M., Chen, Y., Shi, G., Liu, Y., Yang, F., Zhang, L., Deng, L., Yu, J., Peng, C. and
 515 Cao, X.: Seasonal characteristics, formation mechanisms and source origins of PM_{2.5} in two
 516 megacities in Sichuan Basin, China, *Atmos. Chem. Phys.*, 18(2), 865–881, doi:10.5194/acp-18-865-
 517 2018, 2018.
- 518 Wesely, M. L.: Parameterization of surface resistances to gaseous dry deposition in regional-scale
 519 numerical models, *Atmospheric Environment* (1967), 23(6), 1293–1304, doi:10.1016/0004-
 520 6981(89)90153-4, 1989.
- 521 Xu, J., Chang, L., Yan, F. and He, J.: Role of climate anomalies on decadal variation in the
 522 occurrence of wintertime haze in the Yangtze River Delta, China, *Science of The Total Environment*,
 523 599–600, 918–925, doi:10.1016/j.scitotenv.2017.05.015, 2017.
- 524 Xu, X., Zhao, T., Liu, F., Gong, S. L., Kristovich, D., Lu, C., Guo, Y., Cheng, X., Wang, Y. and
 525 Ding, G.: Climate modulation of the Tibetan Plateau on haze in China, *Atmos. Chem. Phys.*, 16(3),



- 526 1365–1375, doi:10.5194/acp-16-1365-2016, 2016.
- 527 Yang, F., Tan, J., Zhao, Q., Du, Z., He, K., Ma, Y., Duan, F., Chen, G. and Zhao, Q.: Characteristics
 528 of PM_{2.5} speciation in representative megacities and across China, *Atmos. Chem. Phys.*, 11(11),
 529 5207–5219, doi:10.5194/acp-11-5207-2011, 2011.
- 530 Zhang, H., Wang, Y., Park, T.-W. and Deng, Y.: Quantifying the relationship between extreme air
 531 pollution events and extreme weather events, *Atmospheric Research*, 1–48,
 532 doi:10.1016/j.atmosres.2016.11.010, 2016.
- 533 Zhang, Q., Streets, D. G., Carmichael, G. R., He, K. B., Huo, H., Kannari, A., Klimont, Z., Park, I.
 534 S., Reddy, S., Fu, J. S., Chen, D., Duan, L., Lei, Y., Wang, L. T. and Yao, Z. L.: Asian emissions
 535 in 2006 for the NASA INTEX-B mission, *Atmos. Chem. Phys.*, 9(14), 5131–5153, doi:10.5194/acp-
 536 9-5131-2009, 2009.
- 537 Zhao, P., Li, Y., Guo, X., Xu, X., Liu, Y., Tang, S., Xiao, W., Shi, C., Ma, Y., Yu, X., Liu, H., Jia,
 538 L., Chen, Y., Liu, Y., Li, J., Luo, D., Cao, Y., Zheng, X., Chen, J., Xiao, A., Yuan, F., Chen, D.,
 539 Pang, Y., Hu, Z., Zhang, S., Dong, L., Hu, J., Han, S. and Zhou, X.: The Tibetan Plateau Surface-
 540 Atmosphere Coupling System and Its Weather and Climate Effects: The Third Tibetan Plateau
 541 Atmospheric Science Experiment, *J Meteorol Res*, 33(3), 375–399, doi:10.1007/s13351-019-8602-
 542 3, 2019.
- 543 Zhao, S., Feng, T., Tie, X., Long, X., Li, G., Cao, J., Zhou, W. and An, Z.: Impact of Climate Change
 544 on Siberian High and Wintertime Air Pollution in China in Past Two Decades, *Earth's Future*, 6,
 545 118–133, doi:10.1002/2017EF000682, 2018.
- 546 Zhao, S., Tie, X., Cao, J. and Zhang, Q.: Impacts of mountains on black carbon aerosol under
 547 different synoptic meteorology conditions in the Guanzhong region, China, *Atmospheric Research*,
 548 164-165(C), 286–296, doi:10.1016/j.atmosres.2015.05.016, 2015.
- 549 Zhu, Q., Shou, S. and Tang, D.: Principles and methods of weather, 4 ed., Beijing, 2000.
- 550 Zou, Y., Wang, Y., Zhang, Y. and Koo, J.-H.: Arctic sea ice, Eurasia snow, and extreme winter haze
 551 in China, *Sci. Adv.*, 3(3), e1602751–9, doi:10.1126/sciadv.1602751, 2017.
- 552



Figure captions

- Figure 1** (a) Location map of the Tibetan Plateau (the region surrounded by the dark line) and the Sichuan Basin (the region surrounded by the gray line). (b) The model domain and the distribution of weather stations marked in the triangles over the Tibetan Plateau and air quality stations marked in the circles over the Sichuan Basin.
- Figure 2** Trends of observational winter (Dec-Jan-Feb) mean temperature anomaly recorded by 10 weather stations over the Tibetan Plateau during the last four decades (1979-2017).
- Figure 3** Trends of ERA-interim reanalysis winter mean temperature over the Tibetan Plateau from 1979 to 2017. The dotted regions show statistical significance with 95% confidence level (p -value < 0.05) from the Student's t test.
- Figure 4** Comparison between the observed (black dots) and simulated (blue line) hourly O_3 ($\mu\text{g m}^{-3}$), CO (mg m^{-3}) and $\text{PM}_{2.5}$ mass concentrations ($\mu\text{g m}^{-3}$) over the Sichuan Basin in January 2014.
- Figure 5** Time series of $\text{PM}_{2.5}$ concentrations over the Sichuan Basin, the baseline simulation is selected in January 2014 and the sensitivity simulation in which 2°C warming occurs over the Tibetan Plateau relative to the baseline simulation.
- Figure 6** Comparison of chemical composition of $\text{PM}_{2.5}$ mass concentrations between the (a) baseline simulation and (b) sensitivity simulation over the Sichuan Basin. The yellow fan-shaped area presents the component of secondary aerosol, and the rest presents primary aerosol.
- Figure 7** Difference in spatial distributions of surface $\text{PM}_{2.5}$ concentrations and winds between the sensitivity simulation and baseline simulation. The negative shows $\text{PM}_{2.5}$ concentrations decrease when the Tibet is 2°C warming, and the positive shows $\text{PM}_{2.5}$ concentrations increase when the Tibet is 2°C warming.
- Figure 8** Spatial change in the PBL height induced by 2°C warming over the Tibet. The positive shows the PBL height increases while the negative shows the PBL height decreases.
- Figure 9** Vertical profiles of changes in temperature (color shading and gray contour) and winds (arrows) along 30°N in January 2014. The gray shaded area presents topography. The green box for the Sichuan Basin, and the red solid (baseline simulation) and dash (sensitivity simulation) lines for the PBL height. (a) The Tibet and Sichuan Basin, and (b) The Sichuan Basin.
- Figure 10** Comparison of spatial distributions of relative humidity (RH) between the (a) baseline simulation and (b) sensitivity simulation over the Tibet and Sichuan Basin.
- Figure 11** Spatial change in the relative humidity after the Tibet becomes 2°C warming. The positive shows the RH increases while the negative shows the RH decreases.

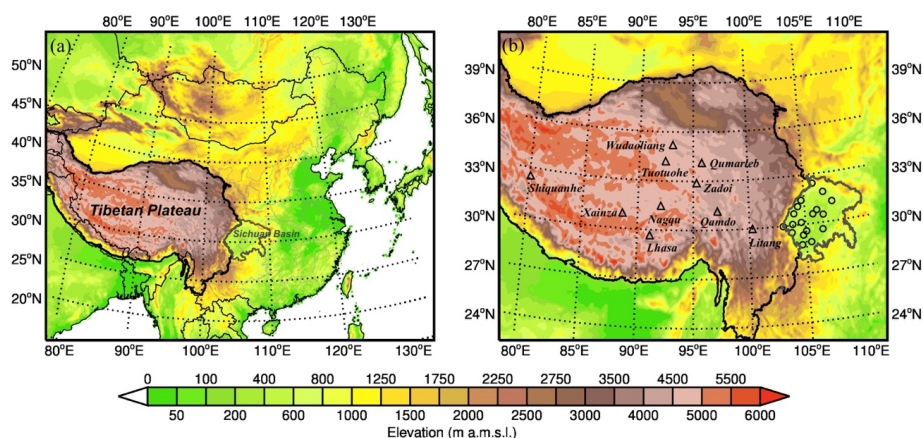


Figure 1 (a) Location map of the Tibetan Plateau (the region surrounded by the dark line) and the Sichuan Basin (the region surrounded by the gray line). (b) The model domain and the distribution of weather stations marked in the triangles over the Tibetan Plateau and air quality stations marked in the circles over the Sichuan Basin.

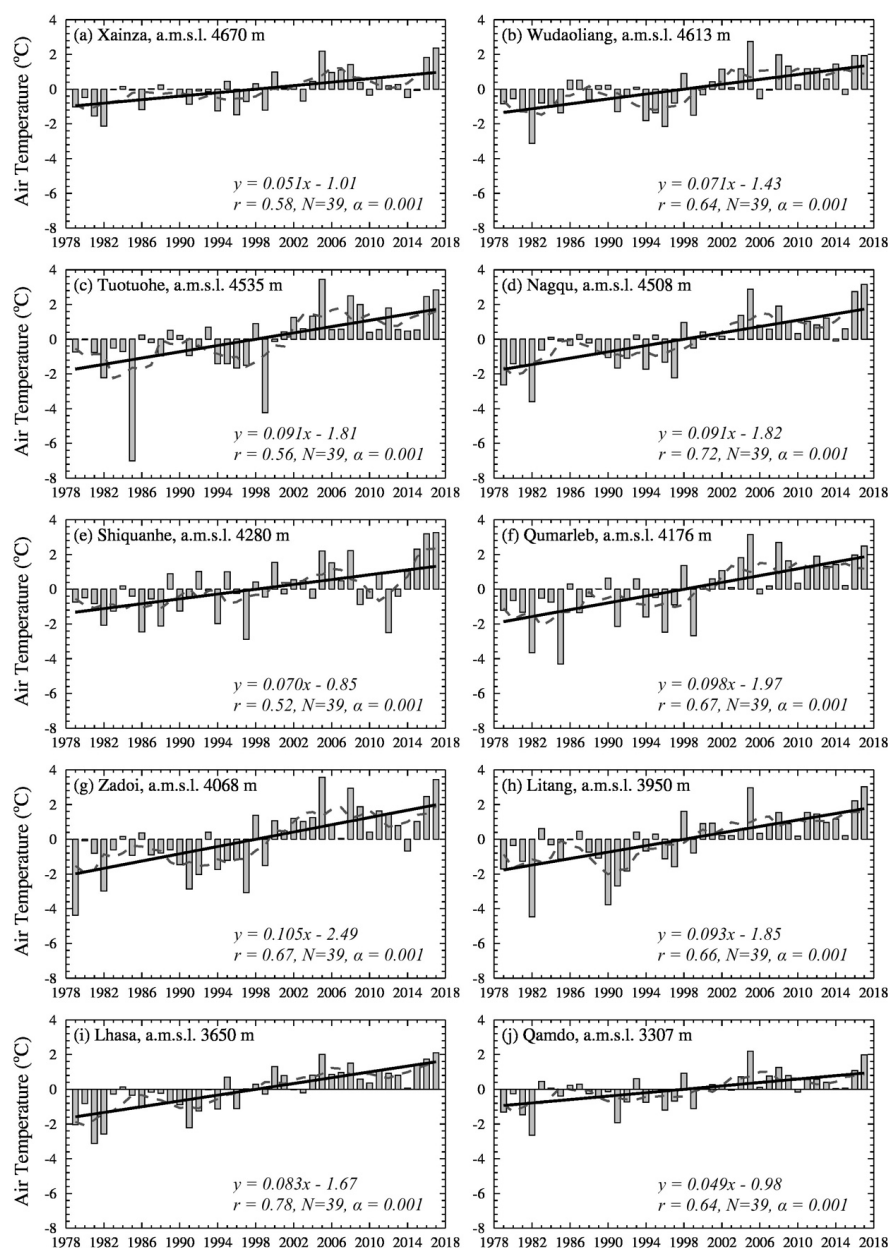


Figure 2 Trends of observational winter (Dec-Jan-Feb) mean temperature anomaly recorded by 10 weather stations over the Tibetan Plateau during the last four decades (1979-2017).

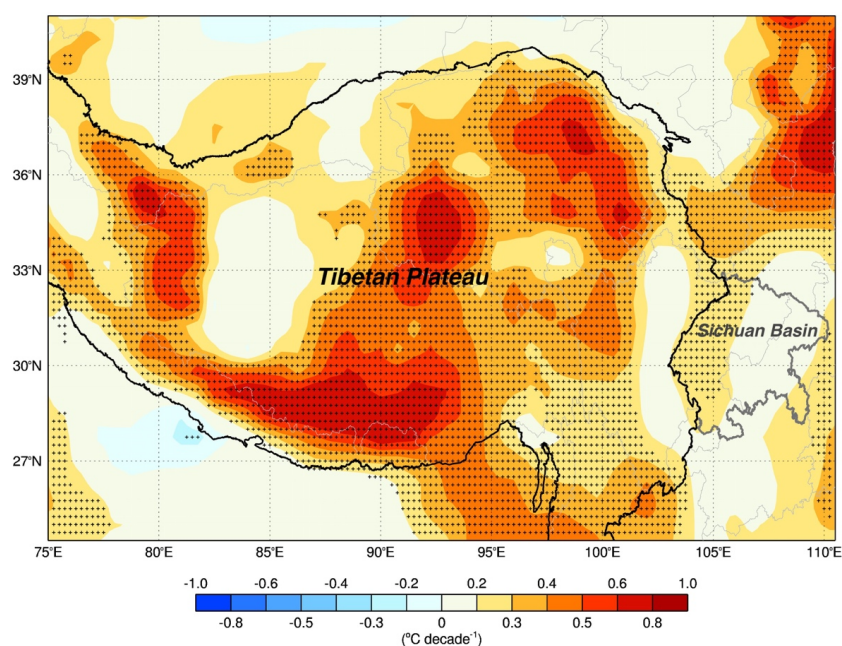


Figure 3 Trends of ERA-interim reanalysis winter mean temperature over the Tibetan Plateau from 1979 to 2017. The dotted regions show statistical significance with 95% confidence level (p -value < 0.05) from the Student's t test.

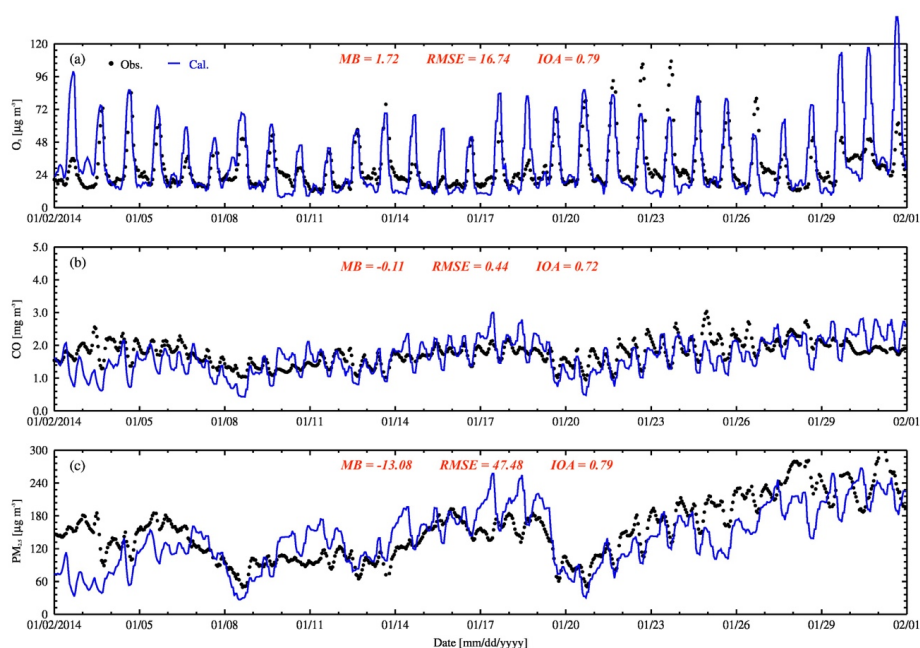


Figure 4 Comparison between the observed (black dots) and simulated (blue line) hourly O_3 ($\mu g m^{-3}$), CO ($mg m^{-3}$) and $PM_{2.5}$ mass concentrations ($\mu g m^{-3}$) over the Sichuan Basin in January 2014.

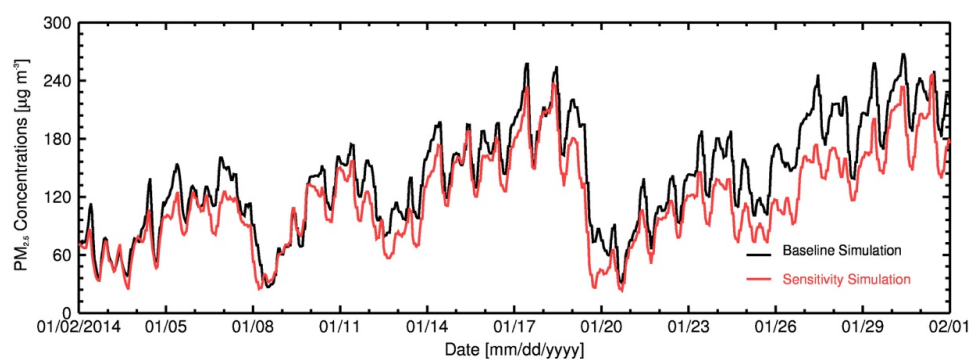


Figure 5 Time series of $\text{PM}_{2.5}$ concentrations over the Sichuan Basin, the baseline simulation is selected in January 2014 and the sensitivity simulation in which 2°C warming occurs over the Tibetan Plateau relative to the baseline simulation.

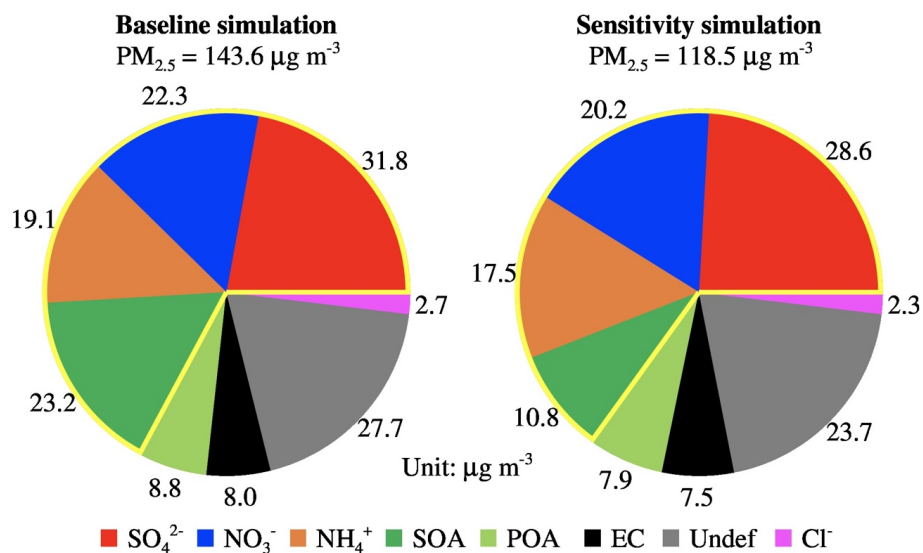


Figure 6 Comparison of chemical composition of $PM_{2.5}$ mass concentrations between the (a) baseline simulation and (b) sensitivity simulation over the Sichuan Basin. The yellow fan-shaped area presents the component of secondary aerosol, and the rest presents primary aerosol.

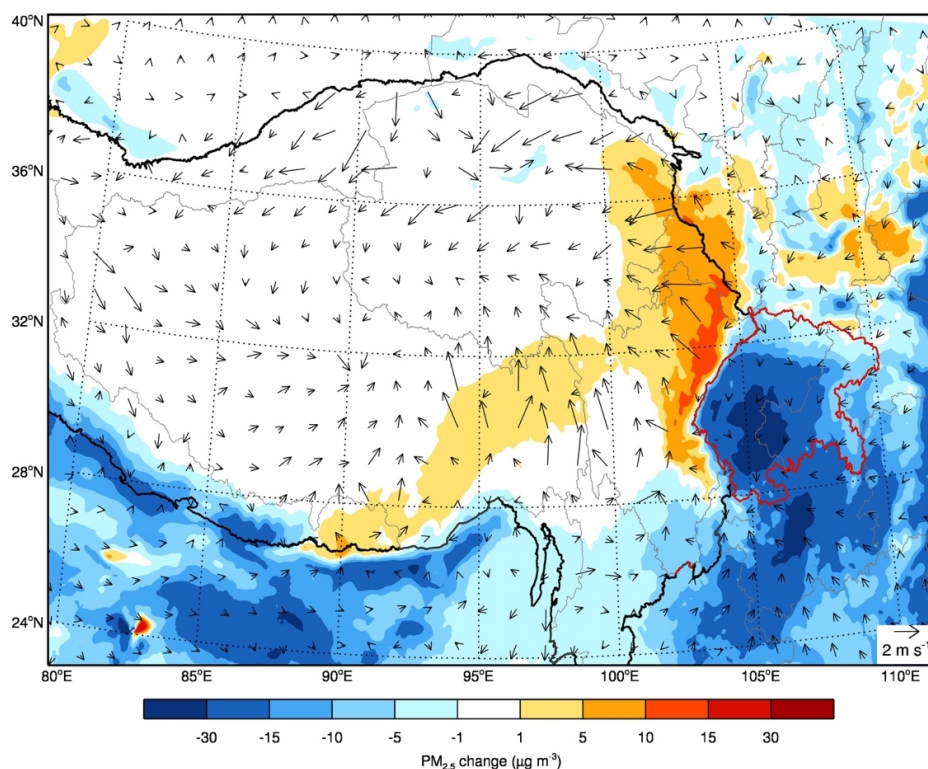


Figure 7 Difference in spatial distributions of surface $\text{PM}_{2.5}$ concentrations and winds between the sensitivity simulation and baseline simulation. The negative shows $\text{PM}_{2.5}$ concentrations decrease when the Tibet is 2°C warming, and the positive shows $\text{PM}_{2.5}$ concentrations increase when the Tibet is 2°C warming.

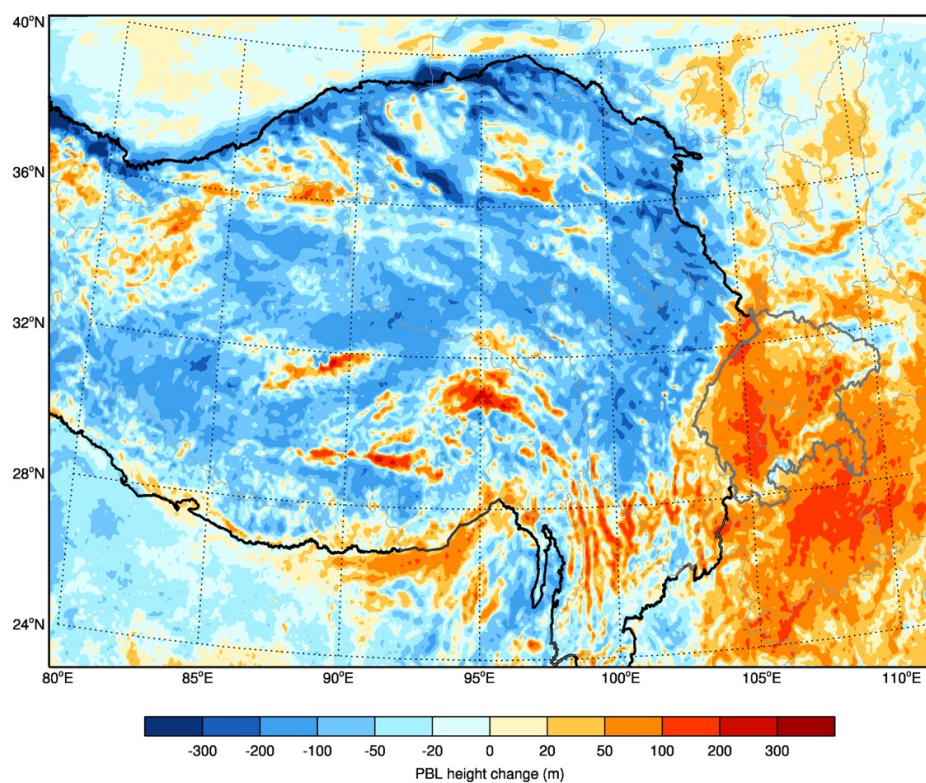


Figure 8 Spatial change in the PBL height induced by 2°C warming over the Tibet. The positive shows the PBL height increases while the negative shows the PBL height decreases.

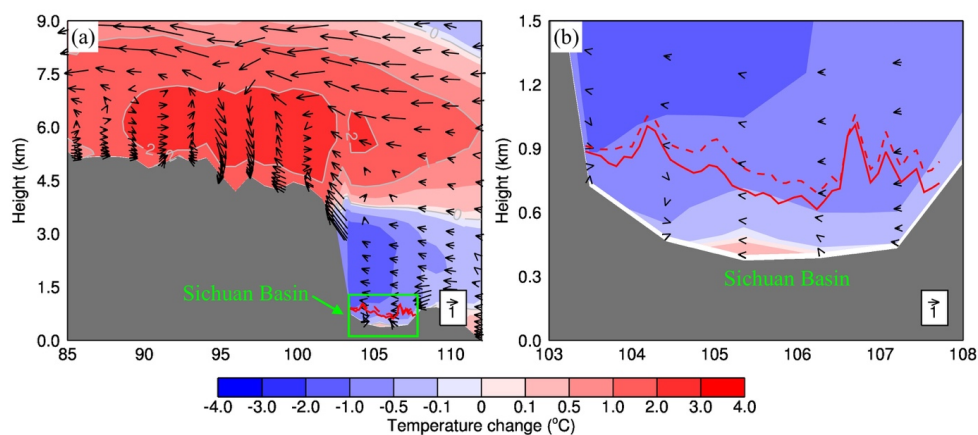


Figure 9 Vertical profiles of changes in temperature (color shading and gray contour) and winds (arrows) along 30°N in January 2014. The gray shaded area presents topography. The green box for the Sichuan Basin, and the red solid (baseline simulation) and dash (sensitivity simulation) lines for the PBL height. (a) The Tibet and Sichuan Basin, and (b) The Sichuan Basin.

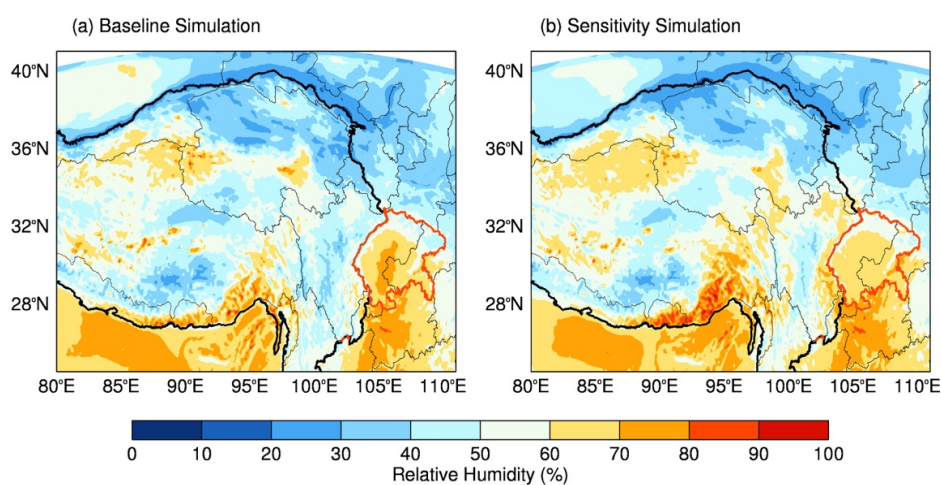
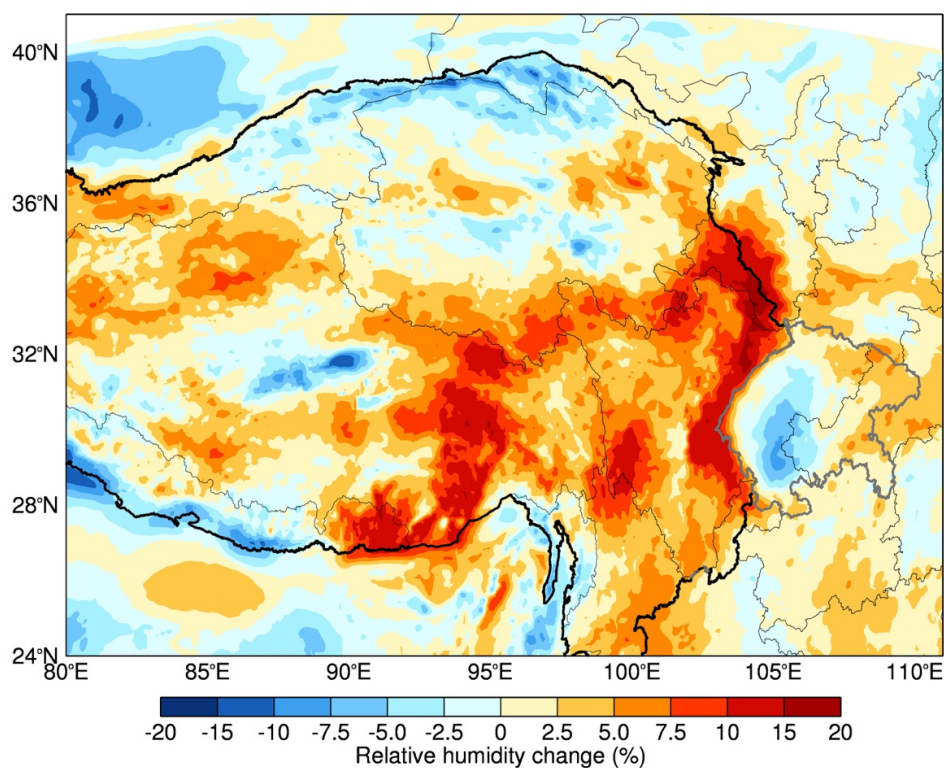


Figure 10 Comparison of spatial distributions of relative humidity (RH) between the (a) baseline simulation and (b) sensitivity simulation over the Tibet and Sichuan Basin.



1



2

3 **Figure 11** Spatial change in the relative humidity after the Tibet becomes 2°C warming. The
 4 positive shows the RH increases while the negative shows the RH decreases.

5

6

7